Environmental Feature Exploration With a Single Autonomous Vehicle

Chiara Mellucci, Prathyush P. Menon, Christopher Edwards, and Peter G. Challenor

***Abstract*— In this paper, a sliding mode-based guidance strategy is proposed for the control of an autonomous vehicle. The aim of the autonomous vehicle deployment is the study of unknown environmental spatial features. The proposed approach allows the solution of both boundary tracking and source-seeking problems with a single autonomous vehicle capable of sensing the value of the spatial field at its position. The movement of the vehicle is controlled through the proposed guidance strategy, which is designed on the basis of the collected measurements without the necessity of preplanning or human intervention. Moreover, no *a priori* knowledge about the field and its gradient is required. The proposed strategy is based on the so-called suboptimal sliding mode controller. The guidance strategy is demonstrated by computer-based simulations and a set of boundary tracking experimental sea trials. The efficacy of the algorithm to autonomously steer the C-Enduro surface vehicle to follow a fixed depth contour in a dynamic coastal region is demonstrated by the results from the trial described in this paper.**

***Index Terms*— Autonomous vehicle, boundary tracking, sliding mode control, source seeking.**

I. Introduction

AUTONOMOUS vehicles have proven to be an effective tool for the study of environmental features and surveying areas characterized by hazardous phenomena [1]. Some of the possible applications of these technologies are: 1) the delineation of polluted regions, such as an ash cloud [2], an oil or chemical spill in the ocean [3], or the extent of a forest fire [4]; 2) the detection of the source of a spreading phenomenon, such as a tracer release [5] or an oil spill; and 3) the enhancement of scientific knowledge, such as the analysis of water properties in tidal mixing front areas [6] or the bathymetric analysis of the ocean seabed [7].

Autonomous vehicles are characterized by low-deployment and operational costs and high endurance, allowing long-term monitoring of the phenomena of interest without direct human intervention or supervision [8]. However, one of the main limitations of modern autonomous vehicle deployments is typically the dependence on preplanning. In most of the up-to-date applications, in fact, despite the availability of on-board computation capabilities, vehicles are operated in a preprogrammed way [9]. Consequently, autonomous vehicles are required to reach a predefined list of *waypoints* [10], which are fixed coordinate points, or to move along a preprogrammed trajectory. Moreover, in most cases, the preplanned motion is through a *lawnmower* or *zig-zag* trajectory [11]. While these environmental sampling strategies allow deep coverage of the considered area, they are associated with high costs in terms of vehicle operation and mission time. Consequently, the creation of improved guidance strategies is necessary for the optimization of sampling and monitoring applications.

Two aspects of interest associated with spatial phenomena are the boundary and the source position, whose study can be translated into guidance objectives, when designing the vehicle control strategy. *Boundary tracking* requires the constant level-sets (boundary) determining the extent of the spatial field to be tracked, while, in *source seeking*, the point associated with the maximum/minimum of the measured quantity, and hence, the source of the spatial phenomenon, is sought. In both cases, knowledge of the spatial field gradient is highly desirable. For example, gradient information is exploited in the virtual body and artificial potential methods [12] and in gradient climbing studies [13]. Spatial derivatives, however, are usually not directly measurable through the vehicle's on-board sensors; consequently, most of the approaches in the literature are based on an estimation procedure. In [14], a formation of vehicles, connected through a communication network, is deployed in order to estimate the gradient of the field and achieve source seeking. Other approaches estimate the field gradient through extremum seeking control techniques [15], by imposing periodic forward–backward movements on the vehicle in order to collect sufficient spatially distributed measurements [16]. The precision of gradient estimates, however, is deteriorated by measurement noise. Moreover, when working with a single vehicle, the estimation of the gradient requires expensive and frequent additional maneuvers or complex hardware design, which results in higher operational costs. Consequently, gradient-free solutions are often preferred. Some of the gradient-free boundary tracking algorithms are the "bang-bang" inspired techniques [17], [18]. A single-vehicle gradient-free boundary tracking algorithm has also been proposed in [2], where the so-called suboptimal sliding mode controller is used to control the direction of movement of the vehicle, provided the initial position of the agent is sufficiently close to the boundary. In addition,

Manuscript received October 11, 2018; accepted February 26, 2019. Date of publication April 30, 2019; date of current version June 11, 2020. Manuscript received in final form March 25, 2019. This work was supported by the Natural Environment Research Council (NERC), the Defense Science and Technology Laboratory (DSTL), and Innovate, U.K., through Phase 2 of the Adaptive Autonomous Ocean Sampling Network (AAOSN) Project (SH-07050). The research data supporting this publication are provided within this paper. Recommended by Associate Editor A. Pavlov. *(Corresponding author: Prathyush P. Menon.)*

The authors are with the College of Engineering, Mathematics and Physical Sciences, University of Exeter, Exeter EX4 4QF, U.K. (e-mail: cm514@exeter.ac.uk; p.m.prathyush@exeter.ac.uk; c.edwards@exeter.ac.uk; p.g.challenor@exeter.ac.uk).

Color versions of one or more of the figures in this article are available online at http://ieeexplore.ieee.org.

Digital Object Identifier 10.1109/TCST.2019.2908141

there exist gradient-free source-seeking algorithms based on sliding mode extremum seeking ideas, see [19], and reactive source-seeking navigation strategies [20].

In this paper, a gradient-free boundary tracking and source-seeking strategy are proposed. The approach is based on a suboptimal sliding mode guidance control strategy, aimed at steering the vehicle to move on the tracked boundary or toward a close neighborhood of the source. The approach makes use of an extremum seeking scheme to find a neighborhood of the maximum/minimum point in the source-seeking application; and a similar strategy is used in the boundary tracking application to find the required contour, in the case, when the vehicle is initially deployed far from it. In contrast to the extremum seeking approach in [19], a 2-D spatial field is considered here. In addition, the slope of the reference trajectory is defined as a function of the sliding variable, rendering it time-varying. A novel design of the reference trajectory is proposed according to the required control objective (boundary tracking or source seeking).

The proposed guidance strategy is initially validated in a synthetic environment through a set of simulations. Subsequently, an embedded unit, supported by a Robot Operating System (ROS) network, is described for testing the proposed approach in a set of field experiments. For the experimental validation, an instrumented autonomous surface vehicle (ASV) has been used with a mission to study an oceanic feature—in this case, the seabed swath bathymetry. However, it should be emphasized that the proposed approach is generic and its application to the study of other environmental spatial features is possible.

The main contributions of this paper are: 1) formulating the problems of boundary tracking and source seeking in a framework that makes use of the so-called suboptimal sliding mode algorithm; 2) a nonlinear guidance strategy that relies only on local measurement of the feature and requires no *a priori* knowledge about the spatial field and its actual or estimated gradient; and 3) bridging the gap between theory and practice by physically implementing the proposed guidance strategy and carrying out an experimental validation of the boundary tracking algorithm at sea.

This paper is organized as follows: the problem considered is formally defined in Section II. The proposed methodology is delineated in Section III, while the embedded system implementation details are overviewed in Section IV. The validation procedure is introduced in Section V: the results of computer-based simulations performed on a synthetic data set are presented in Section V-A, while the pretrials and the sea-trials results are described in Sections V-B and V-C, respectively. Section VI contains the authors' conclusions and some directions for future research.

II. Problem Definition

A. Spatial Phenomenon

In this paper, a spatial phenomenon over a compact 2-D region $\mathcal{D} \subset \mathbb{R}^2$

$$\gamma(x, y) : \mathcal{D} \to \mathbb{R} \tag{1}$$

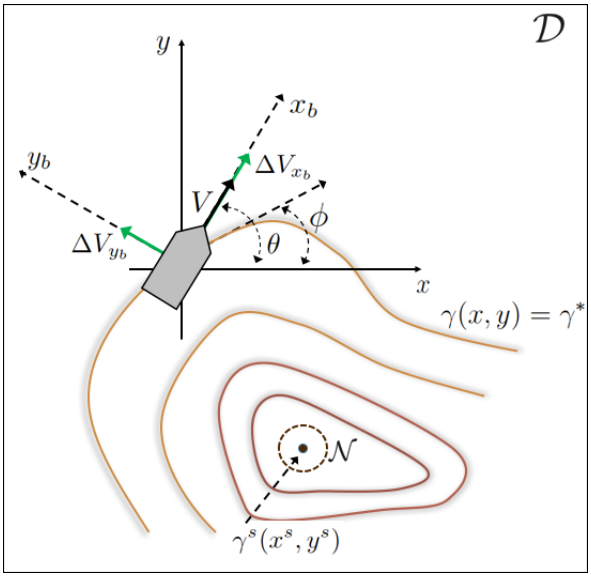

Fig. 1. Spatial field and agent characterization.

is considered. The spatial map $\gamma(x, y)$ associates a measured numerical value of the spatial phenomenon with every position $(x, y) \in \mathcal{D}$. It is assumed that the map has an isolated local maximum

$$\gamma^s(x^s, y^s) = \max_{(x,y)\in\mathcal{D}} \gamma(x, y) \tag{2}$$

located at (x^s, y^s) in the domain $\mathcal{D}$, as shown in Fig. 1, where neither the location of (x^s, y^s) nor the value $\gamma^s(\cdot)$ is known. The boundary of the spatial phenomenon is assumed to be a smooth simple contour, defined as the compact level set

$$\Gamma = \{(x, y) \in \mathcal{D} \mid \gamma(x, y) = \gamma^*\} \tag{3}$$

where $\gamma^* > 0$ is a chosen threshold for the spatial phenomena, representing, for instance, the "safe" contamination level associated with mixing of pollutants in a medium [21]. The temporal evolution of the spatial phenomenon is assumed to be sufficiently slow such that the scenario can be considered static. In contrast to the assumptions in [16] and [22], neither global knowledge of the spatial phenomenon nor the local instantaneous spatial gradient information is assumed to be available or estimated.

In addition, the effects of wind profiles or Lagrangian drift terms are not considered in this paper during the design of the control law. However, their effect is commented on and indeed is present during the sea-trials conducted for the experimental validation of the proposed scheme.

B. Agent Kinematics

A single vehicle is considered and it is assumed to satisfy the nonholonomic kinematics [23]

$$\begin{cases} \dot{x}(t) = V\cos\theta(t) \\ \dot{y}(t) = V\sin\theta(t) \\ \dot{\theta}(t) = u(t) \end{cases} \tag{4}$$

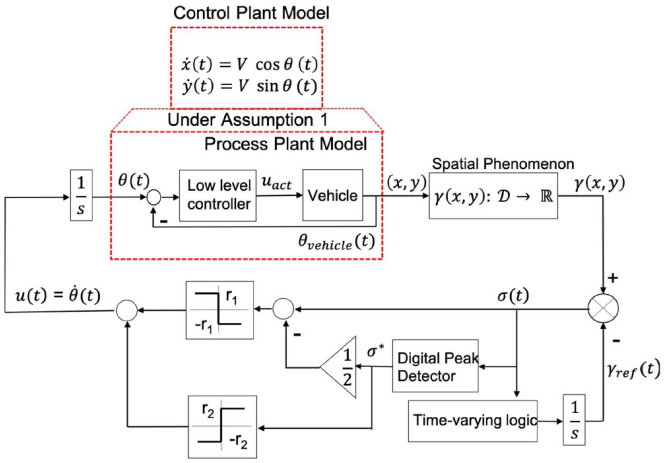

Fig. 2. Schematic of the proposed steering law.

where $x(t)$ and $y(t)$ represent the x-axis and y-axis positions of the agent (e.g., latitude and longitude), and $\theta(t)$ represents the commanded heading angle. The velocity of the vehicle V is assumed constant, while the rate of change of the heading, i.e., the angular velocity, can be directly manipulated through the control law $u(t)$.

Assumption 1: It is assumed that there exists a low-level inner-loop control scheme for the autonomous vehicle, which addresses the motion constraints emanating from the vehicle's dynamics (which have not been precisely accounted for in the proposed approach).

Despite not being an accurate model of the vehicle, the unicycle model is an effective and simple representation of its movement and can be used at the *guidance level*. For example, in [24], a path following guidance strategy is developed based on the kinematic model in (4) and experimentally validated using a small catamaran-like ASV. Similarly, (4) has been used in [2] and [25], for proposing steering laws for an unmanned aerial vehicle moving at a constant height and to design a formation navigation strategy for unmanned ground vehicles (UGVs). A "process plant model" (see [26] for a definition), which encompasses several other aspects of the vehicle dynamics and disturbances present, has been used for validation.

A schematic of the use of the kinematic model in (4) is shown in Fig. 2. The "process plant model" loop is assumed to be a fast internal loop. The aim of this loop is to guarantee, through the low-level controllers, that the actual vehicle's heading coincides with the commanded heading. If the internal loop is fast enough, the commanded and actual heading of the vehicle coincide and the vehicle can be represented by the kinematic unicycle model for designing guidance laws. The commanded heading is obtained by integrating the outer-loop guidance control $u(t)$ in (4). The prime purpose of this paper is to design and validate the guidance control $u(t)$ to meet the objectives listed:

$\mathcal{O}1$ To design a guidance law so that the agent modeled as in (4) identifies and tracks the boundary set Γ.

$\mathcal{O}2$ To design a suitable guidance law so that the agent modeled in (4) climbs the spatial gradient of the feature and reaches a neighborhood of the isolated local maximum in (2) defined as

$$\mathcal{N} := \{(x, y) \in \mathcal{D} : \quad |\gamma(x, y) - \gamma^*| \leq \epsilon\} \tag{5}$$

where $\gamma^* = \gamma(x^*, y^*)$ is the local maximum, and ϵ is a positive constant defining the radius of the neighborhood. If t_s is the time when the vehicle first enters the neighborhood of the source, the vehicle is required to remain inside the neighborhood $\forall t \geq t_s$. In practice, the radius of the neighborhood ϵ is a function of the velocity of the vehicle V and of the nonholonomic constraint, such as the possible minimum turning radius of the vehicle.

III. Methodology

A second-order sliding mode control approach is adopted in this paper to realize $\mathcal{O}1$ and $\mathcal{O}2$. The underlying philosophy of sliding mode control, a popular nonlinear robust control methodology [27], [28], is to first define a manifold, the so-called *sliding surface* [27], and to drive the states of the dynamical system onto the manifold, using an external forcing function (*reaching phase*). Once the states of the system reach the sliding manifold, they are constrained to remain on the sliding surface (*sliding phase*). The sliding surface, representing the desired behavior for the states of the dynamical system, is a function of a *sliding variable*. During the sliding phase, the system shows robustness with respect to the so-called *matched uncertainties* that are uncertainties entering the input channel [27].

Here, the sliding variable is defined as

$$\sigma(t) := \gamma(x(t), y(t)) - \gamma_{\text{ref}}(t) \tag{6}$$

where $\gamma(x(t), y(t))$ is the point measurement of the spatial phenomenon at position $(x(t), y(t))$ as the vehicle traverses within the region $\mathcal{D}$, and $\gamma_{\text{ref}}(t)$ is a (potentially) time-varying reference trajectory. The sliding surface is defined as

$$S := \{(x(t), y(t)) \in \mathcal{D} : \gamma(x(t), y(t)) - \gamma_{\text{ref}}(t) = 0\}. \tag{7}$$

The time-varying reference $\gamma_{\text{ref}}(t)$ depends on the mission objective ($\mathcal{O}1$ or $\mathcal{O}2$).

A. Boundary Tracking

If the mission objective is to identify and track a level set of the spatial phenomenon defined in (3), and represented by γ^*, the choice $\gamma_{\text{ref}}(t) = \gamma^*$ is a possible reference signal. A schematic representation of the proposed guidance law is given in Fig. 2. The vehicle guidance/steering law $u(t)$ in (4) aims to induce a sliding motion on $\sigma(t) = 0$ in finite time. Differentiating $\sigma(t)$ in (6) along the system trajectory (4) yields

$$\begin{aligned}\dot{\sigma}(t) &= \frac{\partial \gamma}{\partial x}(V\cos\theta) + \frac{\partial \gamma}{\partial y}(V\sin\theta) \\ &= V\|\nabla\gamma\|(-\cos\theta\sin(\phi) + \sin\theta\cos(\phi)) \\ &= \|\nabla\gamma\|V\sin(\theta - \phi)\end{aligned} \tag{8}$$

where $\|\nabla\gamma\|$ is the magnitude of the spatial gradient defined as $\nabla\gamma = [(\partial\gamma/\partial x), (\partial\gamma/\partial y)]$, and ϕ is the angle between the tangent line to the tracked contour and the x-axis, as shown in Fig. 1. The projection of the spatial field gradient onto the x- and y- axes yields $(\partial\gamma/\partial x) = -\|\nabla\gamma\|\sin(\phi)$ and $(\partial\gamma/\partial y) = \|\nabla\gamma\|\cos(\phi)$. Since $u(t)$ does not appear explicitly in (8), differentiating once more along the system's trajectory yields

$$\ddot{\sigma}(t) = \underbrace{V\sin(\theta-\phi)\frac{d\|\nabla\gamma\|}{dt}}_{\xi(t)} + \underbrace{\|\nabla\gamma\|V\cos(\theta-\phi)}_{b(t)}(\dot{\theta}-\dot{\phi}). \tag{9}$$

Equation (9) involves a term depending on the vehicle steering law $u(t) = \dot{\theta}(t)$. Consequently, the system between the sliding variable and the control action is relative degree 2 [29]. However, crucially, in (9), the term $\nabla\gamma$ is unknown. The expression in (9) can be written in the following generic form:

$$\ddot{\sigma}(t) = \xi(t) + b(t)(u(t) - \dot{\phi}(t)) \tag{10}$$

where $\xi(t)$ and $b(t)$ are the uncertain time-varying drift and gain terms and $\dot{\phi}(t)$ is treated as *matched uncertainty*. This has an identical structure to the system considered in [28].

To enforce a two-sliding motion [28] in (10), the suboptimal sliding mode steering law

$$u(t) = -r_1\ \text{sign}\left(\sigma - \frac{\sigma^*}{2}\right) + r_2\ \text{sign}(\sigma^*) \tag{11}$$

is employed where the controller gains r_1 and r_2 are the positive design constants, and σ^* is the value of the sliding variable when the condition $\dot{\sigma}(t) = 0$ was last verified [30]. Note that the first derivative of the sliding variable $\dot{\sigma}(t)$ is unknown, as it depends on $\nabla\gamma$ [see (8)]. Hence, the occurrence of a zero-crossing for $\dot{\sigma}(t)$ is determined using a digital peak detector as in [31]. The control law in (11) does *not* require knowledge (or an estimate) of the gradient of the spatial field at the vehicle position. The only necessary information is the field point measurement at the location of the vehicle $\gamma(x(t), y(t))$. According to [28] (among other design constraints), the gains r_1 and r_2 must be chosen so that $r_1 > r_2 > 0$. In particular, it does not require the knowledge of $\dot{\sigma}(t)$.

From the suboptimal sliding mode controller structure in (11), at any point in time

$$u(t) \in \{-r_1 - r_2, -r_1 + r_2, r_1 - r_2, r_1 + r_2\} := \mathcal{R}. \tag{12}$$

During sliding, the control signal will switch at high frequency between these four values [28]. However, if sliding does not occur, then on some time interval $[t_0, t_1]$, $u(t) = r$ where $r \in \mathcal{R}$ is a constant. Then, during the time interval $[t_0, t_1]$, the trajectory of $(x(t), y(t))$ will form part of a circle of radius V/r. This can be justified as follows: for $t \in [t_0, t_1]$, since $\dot{\theta}(t) = u(t) = r$ takes a constant value, it follows from (4) that $\dot{x}(t) = V\cos(rt + \theta_0)$ and $\dot{y}(t) = V\sin(rt + \theta_0)$ where $rt_0 + \theta_0$ corresponds to the heading angle of vehicle at time t_0. It follows by further integration:

$$x(t) = V/r\sin(rt + \theta_0) + x_0 \tag{13}$$

$$y(t) = -V/r\cos(rt + \theta_0) + y_0 \tag{14}$$

where x_0 and y_0 represent the "constants of integration" and depend on $(x(t_0), y(t_0))$. Therefore, $(x(t) - x_0)^2 + (y(t) - y_0)^2 = V^2/r^2$ for $t \in [t_0, t_1]$, which corresponds to circular motion. If the interval $[t_0, t_1]$ is sufficiently long, complete circular motion occurs and a periodic solution emerges.

Suppose, in the subdomain $\bar{\mathcal{D}} \subset \mathcal{D}$ in which the system operates, that $0 < \gamma_0 < \|\nabla\gamma\| < \gamma_1$ and $\max_t \dot{\phi}(t) \le \bar{\phi}$ where γ_0, γ_1, and $\bar{\phi}$ are the positive constants. This implies that there is no local maxima or minima of $\gamma(x, y)$ inside $\bar{\mathcal{D}}$. In this case, the following proposition suggests a choice of gains for r_1 and r_2 and associated conditions under which a two-sliding motion can be attained in (10). [This, in turn, ensures tracking of the contour Γ in (3).] Define three gains C, K_m, and K_M according to the following:

$$C = V(\max_{\bar{\mathcal{D}}}\{\|\nabla^2\gamma\|V\} + \gamma_1\bar{\phi}) \tag{15}$$

$$K_m = \gamma_0 V/15 \tag{16}$$

$$K_M = \gamma_1 V. \tag{17}$$

Proposition 1: Suppose during the motion of the vehicle in $\mathcal{D}$, the "deviation error angle" $|\theta(t) - \phi(t)| < 3/2$ (rads) for all time t, and the controller gains r_1 and r_2 in (11) are chosen so that

$$r_1 - r_2 > \frac{C}{K_m} \tag{18}$$

$$r_1 + r_2 > \frac{(4C + K_M(r_1 - r_2))}{3K_m} \tag{19}$$

then a two-sliding motion is induced in (10) in finite time and the vehicle tracks the contour Γ in (3).

Proof: If $|\theta(t) - \phi(t)| < 3/2$, it is easy to verify (graphically) that $\cos(\theta(t) - \phi(t)) > 1/15$. From (9)

$$\ddot{\sigma}(t) = \underbrace{\xi(t) - b(t)\dot{\phi}(t)}_{\bar{\xi}(t)} + b(t)u(t) \tag{20}$$

and it is easy to verify from the definitions of $\xi(t)$ and $b(t)$ in (9) and the definition of the scalars C, K_m and K_M in (15)–(17) that

$$\begin{aligned}|\xi(t) - b(t)\dot{\phi}(t)| &< V\left(\max_t \frac{d}{dt}\|\nabla\gamma(t)\| + \gamma_1\bar{\phi}\right)\\ &\le (\|\nabla^2\gamma\|V + \gamma_1\bar{\phi})V = C.\end{aligned} \tag{21}$$

Furthermore

$$b(t) = V\|\nabla\gamma\|\cos(\theta(t) - \phi(t)) < V\|\nabla\gamma\| < \gamma_1 V = K_M \tag{22}$$

and

$$b(t) = V\|\nabla\gamma\|\cos(\theta - \phi) > \frac{V\|\nabla\gamma\|}{15} > \frac{V\gamma_0}{15} = K_m > 0. \tag{23}$$

Exploiting the conditions $0 < K_m < b(t) < K_M$, and the norm bound $|\bar{\xi}(t)| < C$, using the result from [28, Th. 4.2, p. 152], it follows $\sigma = \dot{\sigma} = 0$, i.e., a two-sliding motion, is attained in finite time. ■

Remark 1: The constraint that $|\theta(t) - \phi(t)| < 3/2$ (rads) is an assumption, which results in a "local" result. However, it is

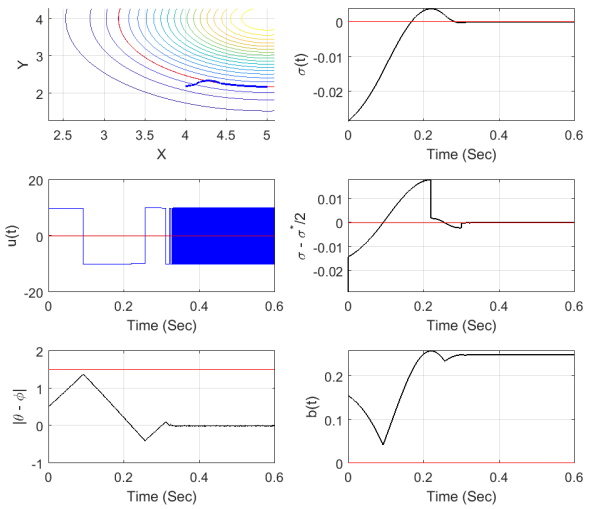

Fig. 3. Simulation results—Case 1.

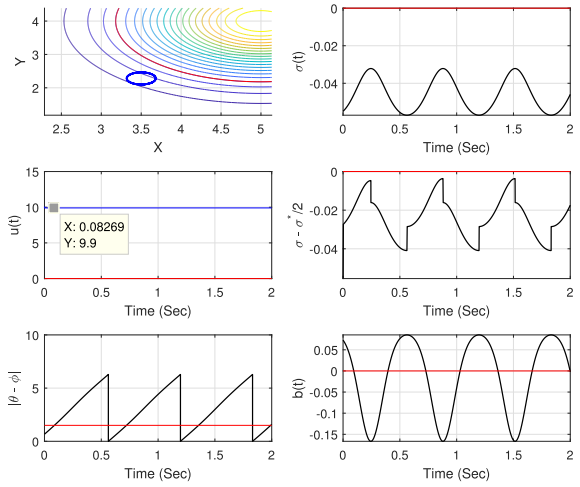

Fig. 4. Simulation results—Case 2.

easy to see from (8) that $\dot{\sigma} = 0$ is equivalent to $\theta(t) = \phi(t)$, and so in a "tube" around the sliding surface when sliding is almost maintained, the deviation error angle condition is intrinsically satisfied.

The most difficult period to ensure $|\theta(t) - \phi(t)| < 3/2$ is in the presliding (reaching) phase, particularly, if $\gamma(0)$ is well away from γ^* at $t = 0$, or if the vehicle is badly misaligned from the required contour. Some simulation examples of these scenarios are shown below on a simple pedagogical example.

B. Pedagogical Example

Consider a Gaussian distribution over a domain $\mathcal{D}$ defined as

$$f(x, y) = \frac{1}{\sqrt{2\pi}} \exp\left(-\frac{(x-\mu_x)^2 + (y-\mu_y)^2}{2}\right) \quad (24)$$

centered at $(\mu_x, \mu_y) = (5, 4)$. The simulations have been run in a MATLAB/Simulink environment (version R 2016b), using a fixed-step Euler integration method, with a step size of 0.1 s. The kinematics of the vehicle with a fixed forward velocity 0.5 m/s $\approx$ 1.8 km/h has been modeled using (4). The angular velocity of (4) has been controlled with the suboptimal sliding mode controller in (11) with gains of $r_1 = 10$ and $r_2 = 0.1$, satisfying (18) and (19).

Case 1: The initial location and orientation for the model in (4), at time $t = 0$, are $(x(0), y(0)) = (4, 2.2)$ and $\theta(0) = 0$. The location is in the vicinity of Γ in (3) where $\gamma^* = 0.075$, which is shown as a red contour in the first subplot of Fig. 3. The occurrence of a typical two-sliding motion, as claimed in [28], can be seen in the $\sigma(t)$ subplot in Fig. 3. At any instant of time, the control input $u(t)$ assumes one of the four values from the set $\mathcal{R}$ in (12). The critical switch (changing polarity in the signal $u(t)$) occurs when the sign of $(\sigma - \sigma^*/2)$ changes and can be seen in the appropriate subplot in Fig. 3. For example, the sign of $(\sigma - \sigma^*/2)$ switches from "negative" to "positive" at 0.1 s. Satisfaction of the "deviation error angle" constraint in Proposition 1, and the resulting positivity of the signal $b(t)$ can be observed, respectively, in the subplots of $|\theta(t) - \phi(t)|$ and $b(t)$.

Case 2: Here, compared to Case 1, a different initial location $(x(0), y(0)) = (3.5, 2.1)$ is considered. All the remaining configurations in the simulation set up are the same as that of Case1. In Case 2, it can be seen that the sign of $(\sigma(t) - \sigma^*/2)$ is negative for the entire simulation period (Fig. 4). Hence, the control $u(t)$ remains unaltered at $r := r_1 - r_2 = 9.9$ and as a consequence, during $[0, 2]$, the trajectory $(x(t), y(t))$, induced by the kinematics in (4), is a circular motion of radius V/r, with the initial deployed location $(x(0), y(0)) = (3.5, 2.1)$ as part of the locus. A two-sliding motion does not occur and the "deviation error angle" condition is periodically violated as shown in the $|\theta - \phi|$ subplot. As a consequence of the variation in $(\theta - \phi)$, the term $b(t)$ changes polarity (and is less than $\gamma_0 V/15$ for a predominant time). In this situation where the polarity of $b(t)$ cannot be maintained positive for a long enough time, all the theoretical developments are no longer valid.

Case 3: This case demonstrates a circular motion followed by the establishment of a two-sliding motion (enabling tracking of the contour). The initial deployment is at $(x(0), y(0)) = (3.473, 2.2)$. Until 0.85 s (see Fig. 5), the scenario identical to that discussed in Case 2 persists, i.e., the vehicle has a circular motion of radius $V/(r_1 - r_2)$. The sign of $(\sigma - \sigma^*/2)$ is negative during the time interval $(0, 0.85)$. At 0.85 s, the sign of $(\sigma - \sigma^*/2)$ changes and the value of $u(t)$ switches from $r_1 - r_2$ (9.9) to $-r_1 - r_2$ (-10.1) [shown in the $u(t)$ subplot], which instigates a prephase of the two-sliding motion. At 1 s, the system enters a regime in which $|\theta(t) - \phi(t)| < 3/2$ rads and consequently $b(t)$ remains positive for the remainder of the simulation and a two-sliding motion is achieved.

Remark 2: Note in Case 3, although the "deviation error angle" condition (which is only a sufficient condition for the establishment of a two-sliding motion) is violated a couple of times, the vehicle recovers and tracks the contour.

C. Modified Reference Profile

To address the problem of initialization and to help to enforce the $|\theta(t) - \phi(t)| < 3/2$ rads "directional error"

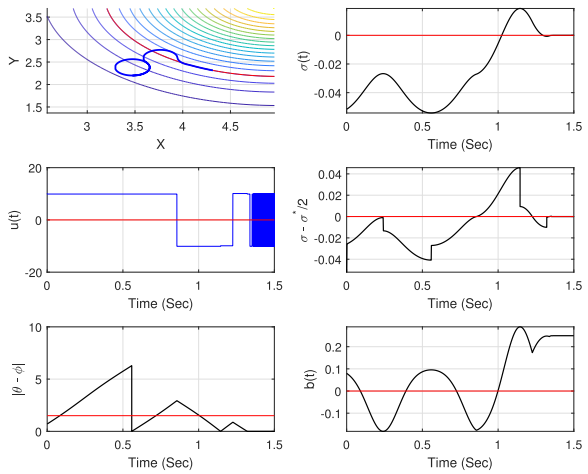

Fig. 5. Simulation results—Case 3.

condition, a modification to the reference signal is proposed. Now, suppose $\gamma_{\text{ref}}(t)$ satisfies

$$\dot{\gamma}_{\text{ref}}(t) = \begin{cases} a_0 \text{sign}(\gamma^* - \gamma(0)), & \text{if } t < \dfrac{|\gamma^* - \gamma(0)|}{a_0} \\ 0, & \text{otherwise} \end{cases} \tag{25}$$

where a_0 is a user-defined positive scalar. In this situation, it can be easily shown that (8) becomes

$$\dot{\sigma}(t) = \|\nabla\gamma\| V \sin(\theta(t) - \phi(t)) - \dot{\gamma}_{\text{ref}} \tag{26}$$

and

$$\begin{aligned} \ddot{\sigma}(t) &= \underbrace{V \sin(\theta - \phi) \frac{d\|\nabla\gamma\|}{dt}}_{\xi(t)} + \underbrace{\|\nabla\gamma\| V \cos(\theta - \phi)}_{b(t)} (\dot{\theta} - \dot{\phi}) \\ &= \underbrace{\xi(t) - b(t)\dot{\phi}(t)}_{\bar{\xi}(t)} + b(t)u(t). \end{aligned} \tag{27}$$

Note from (26), to guarantee a two-sliding motion (in which $\dot{\sigma} = 0$), the condition $a_0 < V\gamma_0$ must hold. This is a design limitation on the choice of a_0. The advantage of this choice of $\gamma_{\text{ref}}(0)$ reference signal is that $\sigma(0) = 0$ and so the evolution starts on the sliding surface [although if $\sin(\phi(0) - \theta(0)) \neq a_0/\|\nabla\gamma(0)\|$ a two-sliding motion, $\sigma(t) = \dot{\sigma}(t) = 0$, will not occur immediately]. The efficacy of this time-varying reference signal can be seen in the following simulations using the pedagogical example.

Pedagogical Example—In the Presence of a Reference Profile: Here Cases 2 and 3, with the initial locations at $(x_0, y_0) = (3.5, 2.1)$ and $(x_0, y_0) = (3.473, 2.2)$, respectively, are reconsidered. The evolution of the trajectory in the xy plane, the sliding variable, the control input, the "deviation error angle," and the uncertain gain term $b(t)$ in the absence of a reference profile were given in Figs. 4 and 5. The reference profile in (25) with a value for $a_0 = 0.1$ has been chosen. This choice satisfies the bound condition $a_0 < \gamma_0 V$. The reference profiles associated with the two cases are given in Fig. 6. Almost identical, improved performance in terms of tracking the boundary Γ, due to the introduction of the reference profiles $\gamma_{\text{ref}}(t)$, can be observed in Figs. 7 and 8. The

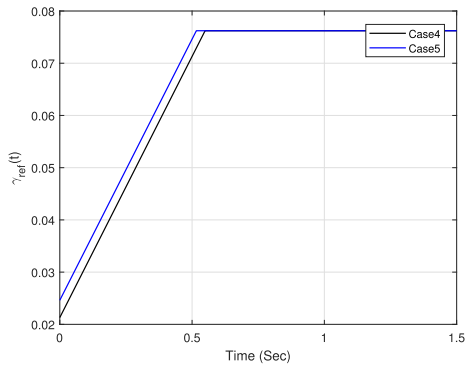

Fig. 6. Reference signal $\gamma_{\text{ref}}(t)$ in Cases 4 and 5.

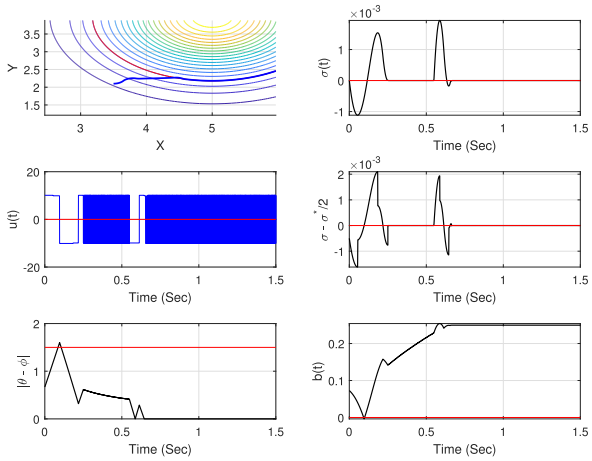

Fig. 7. Simulation results—Case 4.

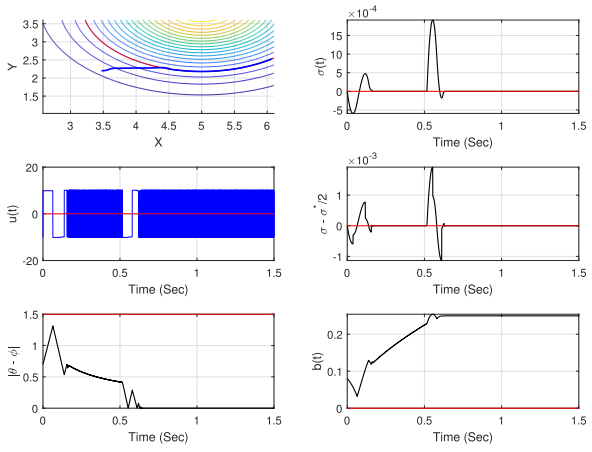

Fig. 8. Simulation results—Case 5.

inherent circular motion behavior which existed previously in both Cases 2 and 3 have been obviated here and the two-sliding motion occurs at 0.66 and 0.63 s, respectively, in Figs. 7 and 8. It should be noted that the "deviation error angle" condition is respected all the time during the simulation and the unknown gain term $b(t)$ is positive and above the bound K_m throughout the simulation.

D. Source Seeking

In this section, it is assumed that a local maximum (source) of $\gamma(.)$ is sought (although the scheme can easily be modified to search for local minima). Now, suppose

$$\dot{\gamma}_{\text{ref}}(t) = \begin{cases} K, & \text{if } |\sigma(t)| < \delta \\ 0, & \text{otherwise} \end{cases} \tag{28}$$

where δ is a small positive scalar chosen to represent sufficiently close behavior to ideal sliding, and the initial condition $\gamma_{\text{ref}}(0) = \gamma(0)$ is applied. Suppose $\bar{\mathcal{D}} \subset \mathcal{D}$ is a proper subdomain containing a single isolated local maxima and the motion of the vehicle is restricted to $\bar{\mathcal{D}}$.

Let $\mathcal{N}$ represent the neighborhood of the local maxima as defined in (5) and consider the motion of the vehicle in $\bar{\mathcal{D}} \setminus \mathcal{N}$. Let C, K_m, and K_M be defined as before in (15)–(17), but now with respect to the domain $\bar{\mathcal{D}} \setminus \mathcal{N}$. Note that because the isolated local maxima does not lie in $\bar{\mathcal{D}} \setminus \mathcal{N}$, $\|\nabla\gamma\| > \gamma_0 > 0$ (although the γ_0 associated with $\bar{\mathcal{D}}$ may be different from the γ_0 associated with $\mathcal{D}$).

Proposition 2: Suppose during the motion of the vehicle in $\bar{\mathcal{D}} \setminus \mathcal{N}$, $|\theta(t) - \phi(t)| < 3/2$ (rad) for all time, and the gains are chosen as in (18) and (19), then the vehicle enters $\mathcal{N}$ (in finite time). Inside $\mathcal{N}$ the two-sliding motion cannot be sustained and the vehicle executes a circular motion in the set $\bar{\mathcal{N}} = \bigcup_{(x,y)\in\mathcal{N}} \mathcal{D}_{xy}$ where $\mathcal{D}_{xy}$ is a disk of radius $V/(r_1 - r_2)$ centered at (x, y).

Proof: As in the proof of Proposition 1, it can be shown

$$\ddot{\sigma}(t) = \underbrace{\xi(t) - b(t)\dot{\phi}(t)}_{\xi(\bar{t})} + b(t)u(t) - \ddot{\gamma}_{\text{ref}}(t). \tag{29}$$

Here, it is assumed, $\ddot{\gamma}_{\text{ref}}(t) = 0$ almost everywhere.[1] Then, as in the proof of Proposition 1, if r_1 and r_2 are chosen such that conditions (18) and (19) from [28, Th. 4.2, p. 152] are satisfied, a two-sliding motion is attained and maintained in finite time. During sliding (provided δ is chosen appropriately), $|\sigma(t)| < \delta$ and so $\dot{\gamma}_{\text{ref}}(t)$ grows monotonically at a rate K as defined in (28). Consequently, $\gamma_{\text{ref}}(t) \to \gamma^*$ and the vehicles enter $\mathcal{N}$. Since $\gamma_{\text{ref}}(t) > \gamma^*$ in finite time, eventually sliding must be broken because once $\gamma_{\text{ref}}(t) > \gamma^*$ then $\sigma(t) < 0$. Once sliding is broken the trajectories $x(t), y(t)$ follow a circular path centered inside $\mathcal{N}$ and the vehicle "loiters" in a region of the point in which the local maximum γ^* occurs—certainly inside the set $\bar{\mathcal{N}} = \bigcup_{(x,y)\in\mathcal{N}} \mathcal{D}_{xy}$. ■

IV. Implementation Details

The suboptimal sliding mode-based approach and the reference trajectory generation discussed in Section III have been implemented in an embedded unit—an ECW 281B computer with Intel Celeron J1900 Processor and an Ubuntu 14.04 operating system which could be placed on the ASV. However, for the first level of experiments, the third party platform was not modified, and the efficacy of the unit was verified in a high-speed Wi-Fi environment. The communication infrastructure makes use of an ROS network [32], which is described in Section IV-A. The algorithms and the ROS network have been developed in C++ and the `roscpp` package [33], respectively.

A. ROS Network

The ROS network that was developed is shown in Fig. 9, which comprises the *nodes*, "UoE Node," "ASVPilot," "Depth Sensor," "Initialization Server," and "ROS Master." The *ROS Master* is the main node of the network, to which the remaining nodes need to register in order to be identified in the network with a unique name and to be able to communicate with other registered nodes. The "UoE Node" represents the embedded unit where the guidance calculations (25), (28), and (11) are carried out to generate the desired steering control command. The "ASVPilot" node is the virtual pilot interface machine between the "UoE Node" and the physical vehicle. The "Depth Sensor" node represents a depth sensor and the "Initialization Server" node allows the user to initialize the control gains r_1, r_2, the trial length and the vehicle's level of thrust.

A node may require to communicate with other nodes to offer its designated functionality. Nodes exchange information through structured data types: ROS *messages*. The communication of an ROS message happens over a *topic*, which is a named bus used for the exchange of a specific type of message. In order to communicate a message, nodes need to publish/subscribe to the corresponding topic. When the node is a publisher to a specific topic, it can communicate information, while it can access any required information by subscribing to the corresponding topic. It is possible to have multiple publishers and/or subscribers for a single topic, and a single node can publish and/or subscribe to multiple topics. The loose coupling inherent in the publisher/subscriber design pattern ensures that the various nodes of the system can be individually developed. It allows quick reconfiguration of the system, as well as the easy implementation of several distributed algorithms [33].

The scheme in Fig. 9 also shows the ROS topics, the ROS services and the role of each node. The "Depth Sensor" node publishes the depth measurement on the corresponding topic. The "ASVPilot" node publishes on the topics relating to the on-board sensors, and in particular, it publishes the position stamp measured through a localization system, the heading, measured through a compass sensor, and the vehicle state (active or paused). The "UoENode" subscribes to a set of topics, in order to access information about the vehicle's position and heading, the vehicle status, and the measured depth. Based on this information, the "UoENode" computes the commanded heading [using (11)] and publishes on the topic corresponding to the manipulated variable. The "ASVPilot" node subscribes to the topic corresponding to the commanded heading, which is made available to the vehicle for use. Every time a new reading is obtained from a sensor, the corresponding message is updated.

[1]The only point at which the gradient of $\gamma_{\text{ref}}(t)$ is undefined is when $|\sigma(t)| = \delta$, elsewhere $\ddot{\gamma}_{\text{ref}}(t) = 0$. Therefore, provided $\dot{\sigma} \neq 0$ when $|\sigma| = \delta$, a motion for which $|\sigma(t)| = \delta$ cannot be sustained and the set of times at which $|\sigma(t)| = \delta$ will have zero measure.

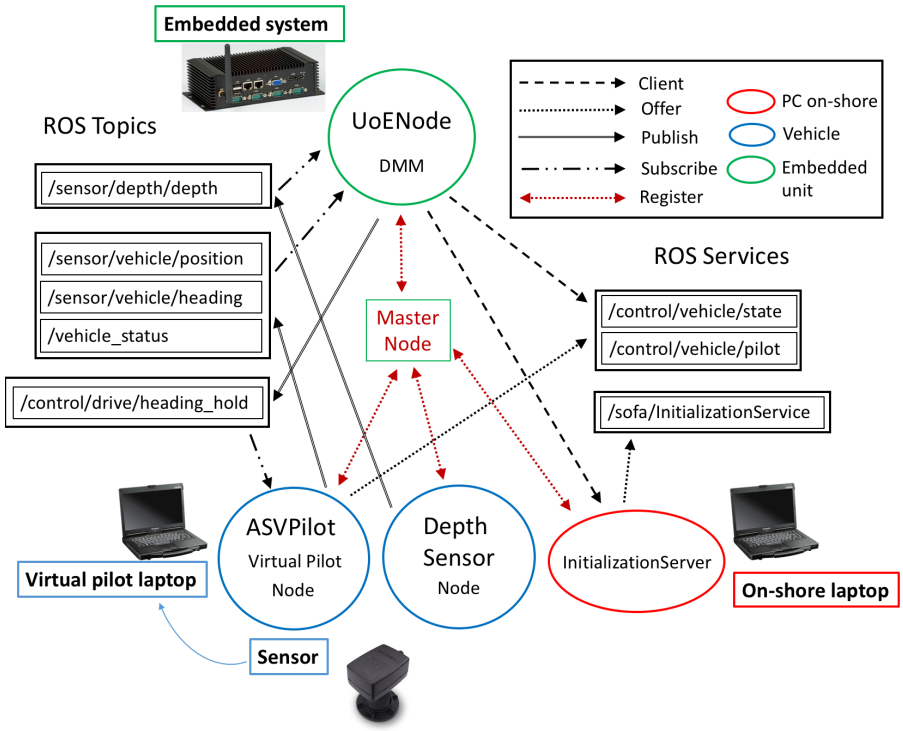

Fig. 9. ROS network.

Despite this fast information update procedure, the "UoE Node" subscription to the topics has been regulated through an *ROS Timer*. Consequently, messages are only read at the timer interrupt instants (every 5 s). Similarly, the "UoE Node" publishes the commanded heading every 5 s, even if the output of the decision-making module is updated less frequently.

V. Results

The proposed methodology has been validated using: 1) a *virtual step*; 2) a set of *hardware in the loop pretrials*; and 3) the final *sea-trials*.

A. Virtual Step

Computer simulations, in a synthetic data-based environment, have been used to test the efficacy of the suboptimal sliding mode guidance approach in (11) for achieving boundary tracking ($\mathcal{O}1$) and source seeking ($\mathcal{O}2$). The synthetic data results used are shown in Figs. 10 and 11 and have been obtained from an available bathymetric image of Ardmucknish Bay, Argyll and Bute, Scotland (56°28′58.1″N − 5°25′54.5″W). Here, the contours correspond to the grayscale color levels representing scaled bathymetric depth.

1) Boundary Tracking Objective: Case 1: An initial position ($t = 0$) for the agent kinematics in (4) has been chosen as $(x(0), y(0)) = (-5.4169, 56.4851)$. The initial heading of the vehicle has been fixed to $\theta(0) = \pi/4, \pi/2$, and $3/4\pi$, respectively, for three different simulations. The vehicle is assumed to move at constant speed $V = 0.5$ m/s. A large minimum turning radius of value $R_{\min} = 60$ m for the vehicle has been assumed.

For determining the gains in (11), the bounds of the uncertainties are assumed to be $C = 25$, $K_m = 10$, and $K_M = 30$. In (11), the gains are set as $r_1 = 28$ and $r_2 = 2$, respectively. The choice of r_1, r_2 respects the assumed minimum turning radius of the vehicle. The parameters relating to the reference trajectory in (25) have been set to $K = 20$, $\delta = 2$, and $\gamma^* = 28$, respectively. The choice of δ fixes the "accepted" tracking error to ± 2, while the chosen slope K determines a slow varying reference trajectory. The vehicle, consequently, is required to find points where the measurements slowly vary from $\gamma(x(0), y(0))$ to γ^*.

Fig. 10(a) (*Case 1* result) shows the trajectories of the vehicle corresponding to the different initial headings $\pi/2, \pi/4$, and $3\pi/4$ in blue, black, and purple, respectively, the initial position of the vehicle as a black star, and the desired contour, characterized by $\gamma(x, y) = 28$, in red. The vehicle successfully reaches the desired contour in finite time and then starts tracking it. Tracking is temporarily lost on two occasions, as highlighted in Fig. 12, where the time evolution of the collected measurements corresponding to the initial condition $\theta(0) = \pi/2$ is shown. The achievable minimum turning radius of the vehicle is higher than the required turning radius for the desired contour as a consequence of the control gains r_1 and r_2.

a) Tuning of the Gains Case 2: Here, the controller gains are increased to $r_1 = 68$, $r_2 = 3$ while keeping the remaining parameters and configuration unchanged. The tracking results are shown in Fig. 11(a). This choice of controller gains reduces the minimum turning radius of the vehicle to $R_{\min} = 25$ m; consequently, as can be seen in Fig. 11(a), the tracking of the contour is improved when compared to that in Fig. 10(a) (especially with regard to the two sharp turns). It can be seen in

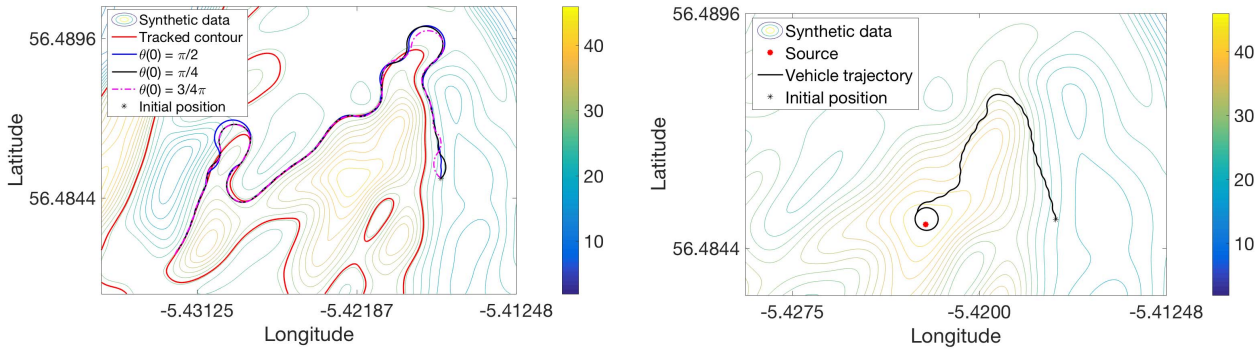

Fig. 10. Synthetic results. (a) Boundary tracking—objective $\mathcal{O}_1$ (Case 1) result. (b) Source seeking—objective $\mathcal{O}_2$ result.

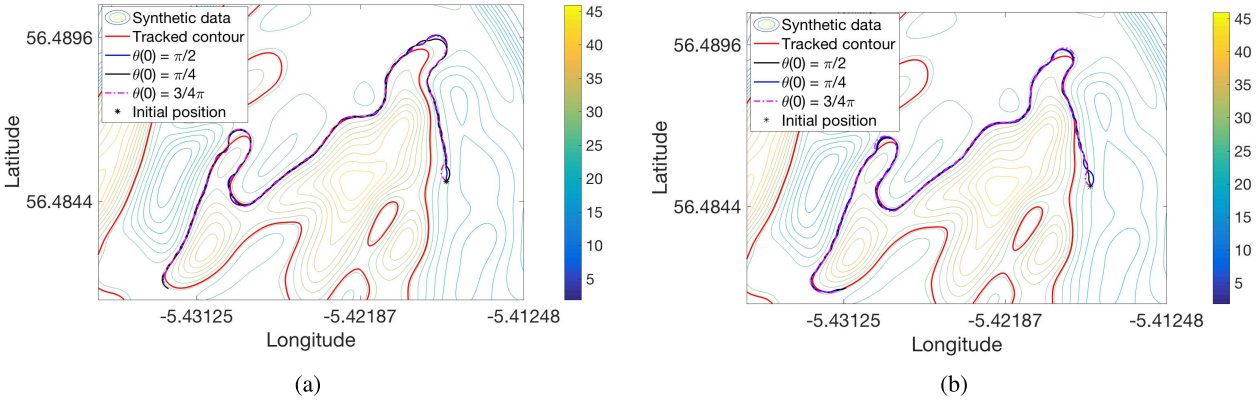

Fig. 11. Synthetic boundary tracking results. (a) Tuning of the gains Case 2. (b) Tuning of the gains Case 3.

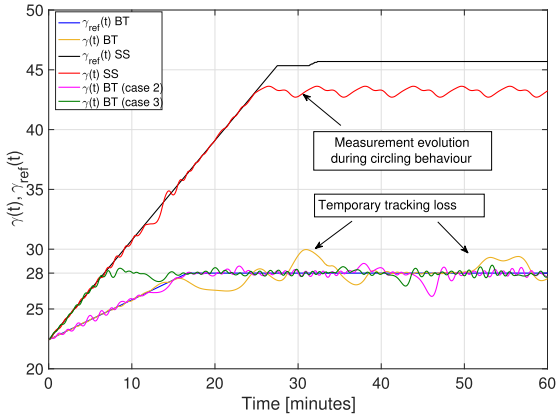

Fig. 12. Reference trajectories and vehicle measurements.

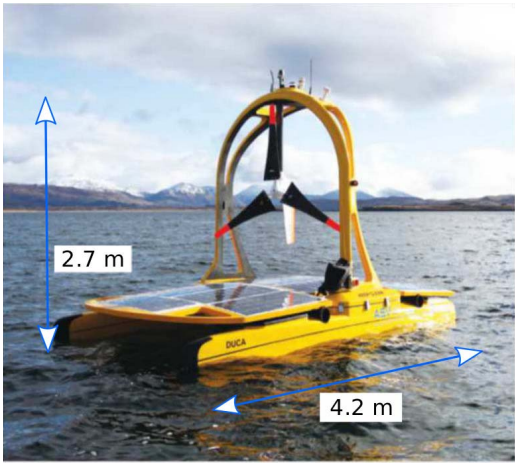

Fig. 13. C-Enduro (Copyright ASV 2015. All rights reserved.).

both Figs. 10(a) and 11(a) that the convergence of the vehicle to the desired contour from the initial position is slow.

b) Tuning of the Gains Case 3: To speed up the convergence to the tracked contour from the vehicle's initial position, the slope parameter of the reference trajectory K is increased to $K = 50$, while $r_1 = 68$ and $r_2 = 3$. As observed in Fig. 11(b), the vehicle quickly moves toward the tracked contour and tight tracking is achieved. The time evolution of the collected measurements in all the cases is shown in Fig. 12 for comparison. It demonstrates how increasing the gains in Case 2 reduces the tracking error, as $\gamma(t)$ tightly tracks the reference trajectory $\gamma_{\text{ref}}(t)$, whereas the modification in Case 3 allows a quicker achievement of the tracked value.

2) Source-Seeking Objective: Now the vehicle is required to determine the position of the point of maximum depth. The simulation parameters, such as the vehicle speed, the simulation time, the drift terms, and the control update frequency

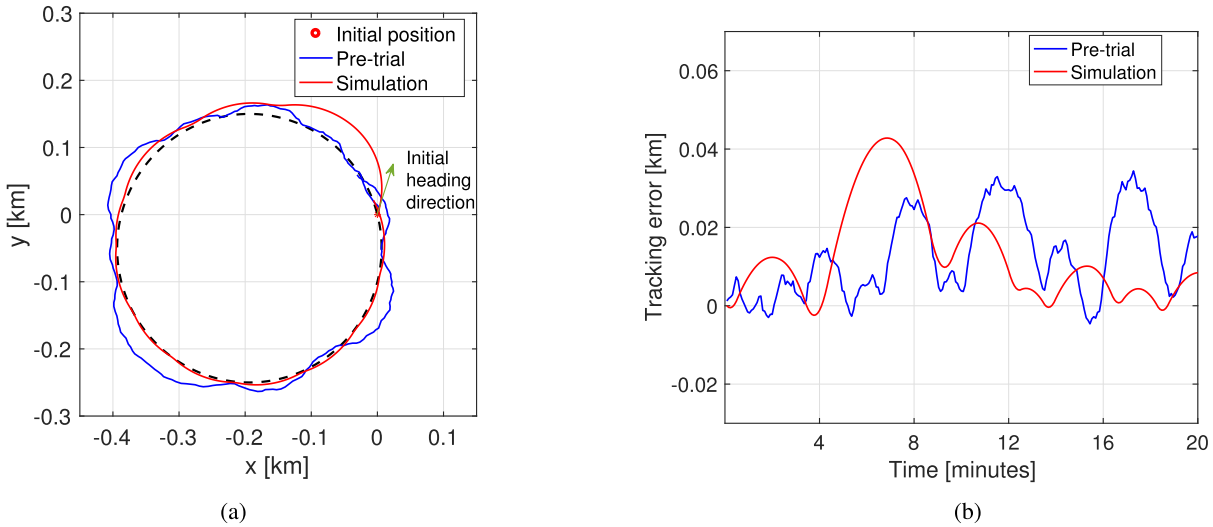

(a) (b)

Fig. 14. Circumference tracking—comparison of the pretrials and simulation results. (a) Pretrial (blue) and simulation (red) trajectories. (b) Comparison of tracking errors.

have been maintained unchanged. To enable the vehicle to undertake a much smaller minimum turning radius, the controller parameters in (11) have been modified as $r_1 = 68$, $r_2 = 3$. Consequently, it is possible for the vehicle to attain a close neighborhood of the source with a small ϵ value of the order of $R_{\min} = 25$ m. The parameters in (28) have been set to $K = 50$ and $\delta = 2$. The slope of the reference trajectory has been set to a greater value, in this case, in order to reduce the time required for the vehicle to reach the neighborhood of the source. The results obtained are shown in Fig. 10(b), where the local maximum is highlighted with a red star. The vehicle successfully moves from its initial position into a neighborhood of the point of maximum depth. Once the neighborhood is entered, it is never left and circling behavior, visible in Fig. 10(b), is obtained. The efficacy of the proposed approach and the robustness of the design in the presence of drift terms are evident from the results. The evolution of the measurements collected during the circling motion around the sought source in $\mathcal{O}2$ and $\gamma_{\text{ref}}(t)$ is shown in Fig. 12.

B. Hardware in the Loop Pretrials

The pretrials had two main motivations: 1) to verify the functionality of the ROS network and the Wi-Fi communication link at sea and 2) to test the performance of the proposed approach in a safe environment, where environmental forces are negligible. The ASV used in the pretrials as well as in the sea trials, shown in Fig. 13, is C-Enduro, developed by ASV Ltd., Portchester, U.K. The vehicle can reach speeds of up to seven knots (approximately 3.5 m/s). A *fixed-thrust* mode, in which the thrust is kept at a constant level independently of the measured speed over ground, is chosen. The vehicle is equipped with an Airmar 200WX and can measure its position through a global navigation satellite system (GNSS), its course over ground, its speed over ground, as well as its roll, pitch, and yaw angles and the wind speed direction. A single beam acoustic depth sensor, characterized by an accuracy of 5 cm, has been chosen for the bathymetry application. The sensor measurements are communicated in National Marine Electronics Association 2000 standard format over the ROS network. The pretrials were conducted partly in Portsmouth Harbor, U.K. ($50°49'52.2''\text{N} - 1°06'59.9''\text{W}$) and partly in Ardmucknish Bay, Argyll and Bute, Scotland ($56°28'58.1''\text{N} - 5°25'54.5''\text{W}$). Initially, the functionality of the communication system was verified by exchanging data over the ROS configuration discussed in Section IV-A.

In the pretrials, the vehicle has been commanded to track a circular contour. In this case, the sliding variable was defined as

$$\sigma(t) = r(t) - R \tag{30}$$

where R is the radius of the tracked circular contour, set to 200 m, and

$$r(t) = \sqrt{(x(t) - x_c)^2 + (y(t) - y_c)^2} \tag{31}$$

is the distance from the current position of vehicle $(x(t), y(t))$ (measured through the GNSS sensor) to the center of the tracked circumference $(x_c, y_c) = (-0.2, -0.05)$. The distance $r(t)$, which is computed onboard, is considered as a virtual range measurement with respect to (x_c, y_c). In order to simplify the task, the vehicle initial position has been considered to be on the tracked circumference.

The thrust of the vehicle has been set equal to 30%, which corresponds to a velocity of approximately 1 m/s. The control gains in (11) have been set to $r_1 = 28$, $r_2 = 2$. With this choice, the vehicle can track contours having a radius of curvature $R > R_{\min} \approx 120$ m, which is significantly bigger than the practical minimum turning radius of C-Enduro, which is of 7 m. Although the "UoE Node" publishes the commanded heading every 5 s, in the pretrials, a new commanded heading is computed and updated only every 30 s. This choice was aimed at assessing the worst case tracking performance.

The results obtained from the pretrials are shown in Fig. 14. The vehicle's trajectory is shown in Fig. 14(a) (blue). The trajectory obtained from a MATLAB-based simulation with an

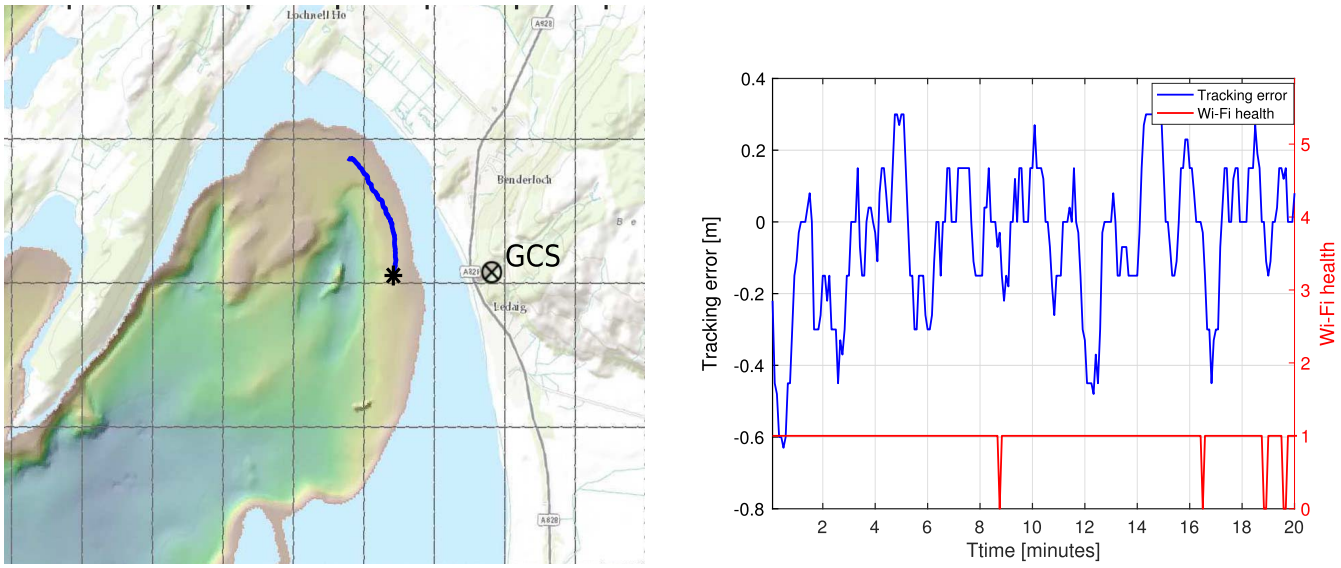

(a) (b)

Fig. 15. Trial result 1—tracking of 12-m-depth contour. (a) Vehicle's trajectory. (b) Tracking error.

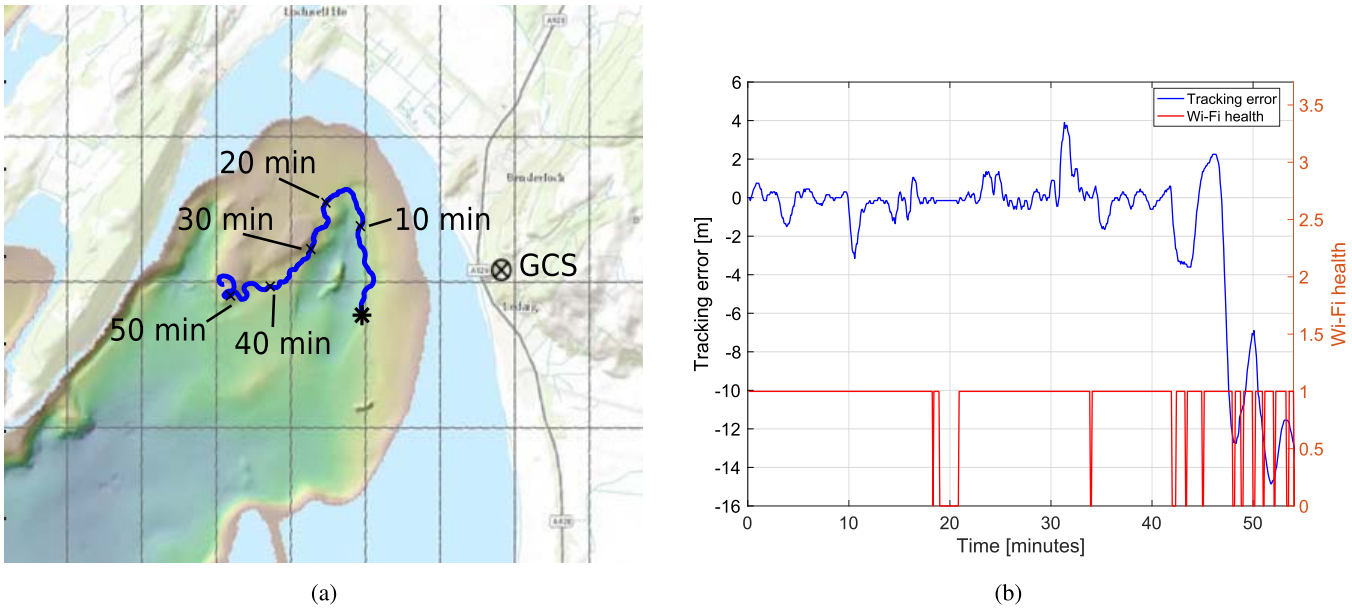

(a) (b)

Fig. 16. Trial result 2—tracking of 20-m-depth contour. (a) Vehicle's trajectory. (b) Tracking error.

identical set up is shown in red for comparison. The tracking errors are depicted in Fig. 14(b). With the chosen control gains and heading update rate, the tracking is reasonable in both the simulated and trial cases. The tracking error is due to the upper bound on the guidance law, due to the gains r_1, r_2, which limit the turning capability of the vehicle as expected. In addition, the deliberate choice of slow update rate (30 s) contributes to the tracking error. The tracking error obtained in the pretrial is comparable, in order of magnitude, to the tracking error obtained from the pure simulation. This shows the effectiveness of the approach and the fidelity of the implementation.

C. Sea Trials Results

Sea trials have been completed in Ardmucknish Bay off Dunstaffnage in Scotland (56°28′58.1″N−5°25′54.5″W) [34].

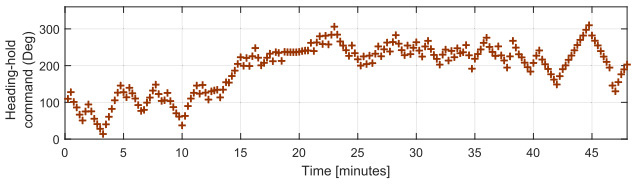

Fig. 17. Trial result 2—heading-hold commands to vehicle.

This is an area which benefits from low sea traffic, depth contours in the range of 5–30 m all along the bay, and access to available support facilities including a slipway for the launch and recovery of the vehicle. The Ground Control Station (GCS), indicated in Fig. 15(a) as an encircled black cross, is the on-shore location, where the embedded computer,

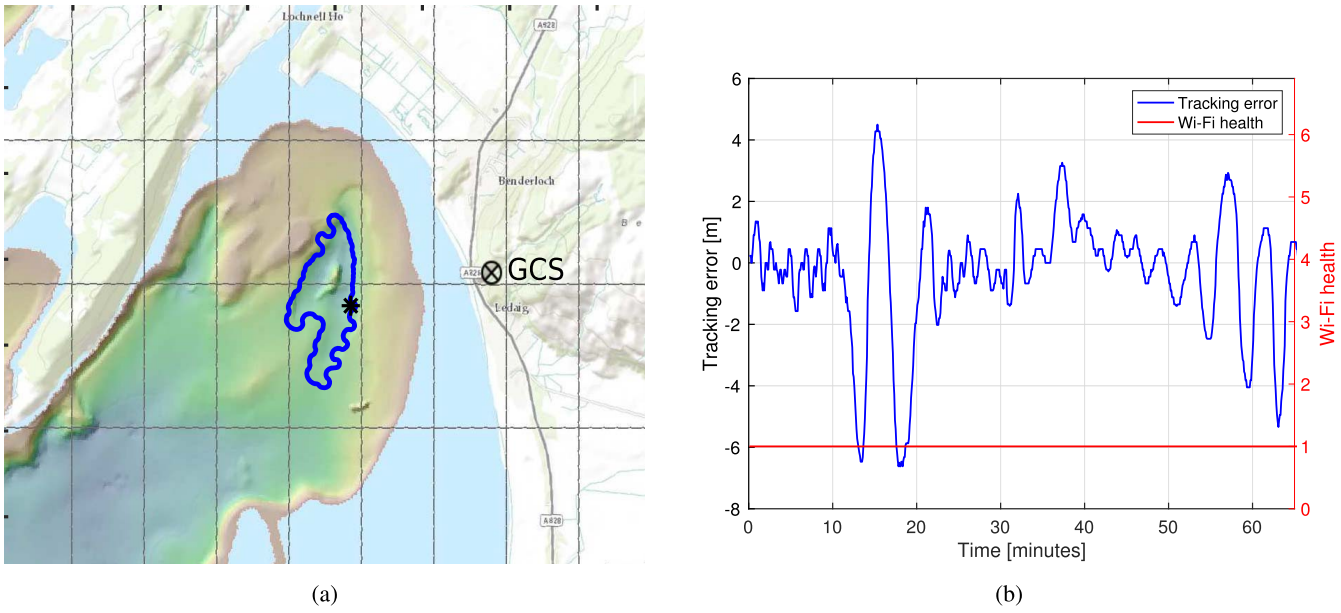

(a) (b)

Fig. 18. Trail result 3—tracking of 32-m-depth closed contour. (a) Vehicle's trajectory. (b) Tracking error.

the Virtual Pilot laptop, and the Wi-Fi antenna have been set up. The bay in front of the GCS has a sweep of approximately 3 km, which is greater than the range of the directional Wi-Fi antenna used (of the order of 2 km).

During the sea trials, the vehicle has been operated in the *fixed thrust* mode, with the level of thrust fixed at the 20%. This corresponds to a speed of approximately 0.7 m/s. The controller gains in (11) have been kept the same as in the pretrials, $r_1 = 28, r_2 = 2$. Because of the lower speed, this configuration allows the vehicle to track contours having a radius of curvature $R > R_{\min} \approx 90$ m. The commanded heading for the actuators of the vehicle has been updated at fixed intervals of 15 s.

1) Trial Result 1: In the sea trial shown in the bathymetric image in Fig. 15, the vehicle was commanded to track a depth contour of $\gamma^* = 12$ m. The trajectory of the C-Enduro on the bathymetry image of Ardmucknish Bay is shown in Fig. 15(a). The initial position is indicated as a black star. In the bathymetric image, the color scale represents the water depth, and the full range of the scale is between 0 and 50 m. Fig. 15(b) shows the tracking error, defined as the difference between the depth measurements collected at the vehicle position over time and the tracked depth (12 m), i.e., the value of the switching function $\sigma(t)$. The tracking error is, in absolute value, smaller than 0.5 m for the entire duration of the trial, showing the effectiveness of the proposed approach.

2) Trial Result 2: In this case, the C-Enduro vehicle was commanded to track a contour of depth 20 m, i.e., $\gamma^* = 20$ m. The configuration, the values of controller gains and the thrust level, is identical to Trial 1. The trajectory that the vehicle followed is indicated in Fig. 16(a). The heading-hold command (in degree) at fixed intervals of 15 s is given in Fig. 17, enabling the vehicle to follow the trajectory shown in Fig. 16(a). The depth variations in the seabed along the trajectory are evident from the variations in the color scale of the bathymetric image in Fig. 16(a). Considering the steepness of the seabed in the area of the tracked contour, the tracking error, shown in Fig. 16(b), is very satisfactory, being less than 1 m in absolute value for most of the duration of the trial (up to 45 min) with the exception of a few peaks, in which it is still less than 4 m. These excursions occur for two main reasons: 1) the curvature of the tracked contour and 2) Wi-Fi dropouts. The Wi-Fi health signal is shown in Fig. 16(b) (red), where the value of 0 and 1 indicates the absence and presence of Wi-Fi, respectively. Temporary Wi-Fi dropouts, at approximately 35 and 42 min, affect tracking. From 48 min onward, when the vehicle is on the boundary of the 2-km Wi-Fi antenna range, several Wi-Fi dropouts are observed, which deteriorate the tracking performance. Embedding the methodology on-board would remove the dependence on the Wi-Fi communication and avoid any performance loss in tracking.

3) Trial Result 3: A final set of sea trials results is shown in Fig. 18. In this trial, the vehicle was required to track a closed contour, characterized by $\gamma^* = 32$ m. The vehicle's trajectory, in Fig. 18(a), shows how the vehicle successfully tracks the complete closed contour in an anticlockwise direction. The tracking error is shown in Fig. 18(b). After approximatively 10 min, the tracking error shows some oscillations: these are due to the abrupt change in the direction of the contour as it approaches the end of the "canyon." The vehicle loses tracking temporarily and it has to turn back in order to recover. This causes an almost 90° cross cut of the tracked contour, and a consequent second overshoot. The succession of overshoots is continuously reduced in amplitude, until tracking of the contour is regained. In fact, such behavior is a feature of the suboptimal algorithm [28].

The second difficulty encountered during this trial is due to the absence of many points in which the water was 32 m deep in the bottom-right part of the trajectory. After approximately 50 min, the vehicle starts oscillating around the contour again, but every time that the contour is lost, it is successfully

regained after a few oscillations. This highlights the capability of the algorithm to successfully recover tracking. The overall tracking error is smaller than 5 m in absolute value for the whole duration of the trial and this has been judged to be satisfactory, especially considering the difficulty level of this trial. The presence of external environmental forces, such as wind, water currents, and tides, needs to be accounted for in each of the trials. The results obtained prove that high performance is obtainable with the proposed guidance strategy and highlight the robustness of the approach to (a certain level) of external disturbances.

VI. Conclusion

The sea trials results presented in this paper demonstrate the effectiveness of a suboptimal sliding mode-based guidance strategy. Novel reference trajectory generation is employed in the proposed guidance scheme to tackle two distinct autonomous behaviors such as boundary tracking and source seeking. The methodology was implemented in an embedded unit supported by the ROS, which is a metaoperating system. The framework has been tested in a Wi-Fi-enabled experiment. The application described in the paper represents a step toward the use of autonomous vehicles equipped with on-board intelligence, which do not require a preplanned trajectory but are able to determine their trajectories autonomously and efficiently learn about the oceanic features. In future, the implementation will be developed further to integrate with third-party autonomous vehicles in a plug-and-play manner.

Acknowledgment

The authors would like to thank Autonomous Surface Vehicles (ASV) Ltd., Portchester, for the support during the sea trials. They would also like to thank Prof. G. Griffiths and J. Holmes (JHC Ltd.) for the support throughout the project.

References

[1] M. Dunbabin and L. Marques, "Robots for environmental monitoring: Significant advancements and applications," *IEEE Robot. Autom. Mag.*, vol. 19, no. 1, pp. 24–39, Mar. 2012.

[2] P. P. Menon, C. Edwards, Y. B. Shtessel, D. Ghose, and J. Haywood, "Boundary tracking using a suboptimal sliding mode algorithm," in *Proc. 53rd Conf. Decision Control (CDC)*, Dec. 2014, pp. 5518–5523.

[3] Y. Cao and R. Fierro, "Dynamic boundary tracking using dynamic sensor nets," in *Proc. 45th Conf. Decision Control (CDC)*, Dec. 2006, pp. 703–708.

[4] D. W. Casbeer, D. B. Kingston, R. W. Beard, and T. W. McLain, "Cooperative forest fire surveillance using a team of small unmanned air vehicles," *Int. J. Syst. Sci.*, vol. 37, no. 6, pp. 351–360, 2006.

[5] C. Mellucci, P. P. Menon, C. Edwards, and P. Challenor, "Source seeking using a single autonomous vehicle," in *Proc. Amer. Control Conf. (ACC)*, Jul. 2016, pp. 6441–6446.

[6] J. Holt and L. Umlauf, "Modelling the tidal mixing fronts and seasonal stratification of the Northwest European Continental shelf," *Continental Shelf Res.*, vol. 28, no. 7, pp. 887–903, 2008.

[7] A. Y. Shcherbina, G. G. Gawarkiewicz, C. A. Linder, and S. R. Thorrold, "Mapping bathymetric and hydrographic features of Glover's reef, Belize, with a REMUS autonomous underwater vehicle," *Limnol. Oceanogr.*, vol. 53, no. 5, pp. 2264–2272, 2008.

[8] A. S. Matveev, H. Teimoori, and A. V. Savkin, "A method for guidance and control of an autonomous vehicle in problems of border patrolling and obstacle avoidance," *Automatica*, vol. 47, no. 3, pp. 515–524, 2011.

[9] N. E. Leonard, D. A. Paley, F. Lekien, R. Sepulchre, D. M. Fratantoni, and R. E. Davis, "Collective motion, sensor networks, and ocean sampling," *Proc. IEEE*, vol. 95, no. 1, pp. 48–74, Jan. 2007.

[10] E. Fiorelli, P. Bhatta, N. E. Leonard, and I. Shulman, "Adaptive sampling using feedback control of an autonomous underwater glider fleet," in *Proc. 13th Int. Symp. Unmanned Untethered Submersible Technol. (UUST)*, 2003, pp. 1–16.

[11] R. N. Smith, Y. Chao, P. P. Li, D. A. Caron, B. H. Jones, and G. S. Sukhatme, "Planning and implementing trajectories for autonomous underwater vehicles to track evolving ocean processes based on predictions from a regional ocean model," *Int. J. Robot. Res.*, vol. 29, no. 12, pp. 1475–1497, 2010.

[12] P. Ögren, E. Fiorelli, and N. E. Leonard, "Cooperative control of mobile sensor networks: Adaptive gradient climbing in a distributed environment," *IEEE Trans. Autom. Control*, vol. 49, no. 8, pp. 1292–1302, Aug. 2004.

[13] R. Bachmayer and N. E. Leonard, "Vehicle networks for gradient descent in a sampled environment," in *Proc. 41st Conf. Decision Control (CDC)*, 2002, pp. 112–117.

[14] L. Briñón-Arranz, A. Seuret, and C. Canudas-de-Wit, "Collaborative estimation of gradient direction by a formation of auvs under communication constraints," in *Proc. 50th IEEE Conf. Decision Control Eur. Control Conf. (CDC-ECC)*, Dec. 2011, pp. 5583–5588.

[15] S.-J. Liu and M. Krstic, "Introduction to extremum seeking," in *Stochastic Averaging and Stochastic Extremum Seeking*. London, U.K.: Springer, 2012, pp. 11–20.

[16] J. Cochran and M. Krstic, "Nonholonomic source seeking with tuning of angular velocity," *IEEE Trans. Autom. Control*, vol. 54, no. 4, pp. 717–731, Apr. 2009.

[17] Z. Jin and A. L. Bertozzi, "Environmental boundary tracking and estimation using multiple autonomous vehicles," in *Proc. 46th Conf. Decision Control (CDC)*, Dec. 2007, pp. 4918–4923.

[18] A. Joshi, T. Ashley, Y. R. Huang, and A. L. Bertozzi, "Experimental validation of cooperative environmental boundary tracking with on-board sensors," in *Proc. Amer. Control Conf. (ACC)*, Jun. 2009, pp. 2630–2635.

[19] Y. Pan, K. D. Kumar, and G. Liu, "Extremum seeking control with second-order sliding mode," *SIAM J. Control Optim.*, vol. 50, no. 6, pp. 3292–3309, 2012.

[20] A. S. Matveev, M. C. Hoy, and A. V. Savkin, "Extremum seeking navigation without derivative estimation of a mobile robot in a dynamic environmental field," *IEEE Trans. Control Syst. Technol.*, vol. 24, no. 3, pp. 1084–1091, May 2016.

[21] J.-S. Kim, P. P. Menon, J. Back, and H. Shim, "Disturbance observer based boundary tracking for environment monitoring," *J. Elect. Eng. Technol.*, vol. 12, no. 3, pp. 1299–1306, 2017.

[22] C. Zhang, D. Arnold, N. Ghods, A. Siranosian, and M. Krstic, "Source seeking with non-holonomic unicycle without position measurement and with tuning of forward velocity," *Syst. Control Lett.*, vol. 56, no. 3, pp. 245–252, 2007.

[23] G. Indiveri, "Kinematic time-invariant control of a 2D nonholonomic vehicle," in *Proc. 38th IEEE Conf. Decision Control (CDC)*, Dec. 1999, pp. 2112–2117.

[24] M. Bibuli, G. Bruzzone, M. Caccia, and L. Lapierre, "Path-following algorithms and experiments for an unmanned surface vehicle," *J. Field Robot.*, vol. 26, no. 8, pp. 669–688, 2009.

[25] H. Teimoori and A. V. Savkin, "Equiangular navigation and guidance of a wheeled mobile robot based on range-only measurements," *Robot. Auton. Syst.*, vol. 58, no. 2, pp. 203–215, 2010.

[26] A. J. Sørensen, "Structural issues in the design and operation of marine control systems," *Annu. Rev. Control*, vol. 29, no. 1, pp. 125–149, 2005.

[27] C. Edwards and S. Spurgeon, *Sliding Mode Control: Theory And Applications*. Boca Raton, FL, USA: CRC Press, 1998.

[28] Y. Shtessel, C. Edwards, L. Fridman, and A. Levant, *Sliding Mode Control and Observation*. New York, NY, USA: Birkhäuser, 2014.

[29] H. K. Khalil, *Nonlinear Systems*. Upper Saddle River, NJ, USA: Prentice-Hall, 1996.

[30] G. Bartolini, A. Ferrara, and E. Usai, "Chattering avoidance by second-order sliding mode control," *IEEE Trans. Autom. Control*, vol. 43, no. 2, pp. 241–246, Feb. 1998.

[31] G. Bartolini, A. Pisano, and E. Usai, "Digital second-order sliding mode control for uncertain nonlinear systems," *Automatica*, vol. 37, no. 9, pp. 1371–1377, 2001.

[32] M. Quigley *et al.*, "ROS: An open-source Robot Operating System," in *Proc. ICRA Workshop Open Source Softw.*, 2009, vol. 3, no. 2, pp. 5–10.

[33] J. M. O'Kane, "A gentle introduction to ROS," Univ. South Carolina, Columbia, SC, USA, 2014.

[34] C. Mellucci, P. P. Menon, C. Edwards, and P. Challenor, "Experimental validation of boundary tracking using the suboptimal sliding mode algorithm," in *Proc. Amer. Control Conf. (ACC)*, May 2017, pp. 4878–4883.

Chiara Mellucci received the B.S. degree (Hons.) in industrial engineering and the M.S. degree (Hons.) in electrical engineering from the University of Pavia, Pavia, Italy, in 2012 and 2014, respectively. She is currently pursuing the Ph.D. degree in mathematics with the University of Exeter, Exeter, U.K. Her current research interests include control strategies for autonomous vehicles deployed to explore environmental features.

Prathyush P. Menon is currently an Associate Professor of control systems with the College of Engineering, Mathematics and Physical Sciences, University of Exeter, Exeter, U.K. His current research interests include control, sliding mode observers, multiagent systems, optimization, and simulation-based robustness analysis and uncertainty quantification. He has authored 100 refereed papers in these areas, including 35 journal publications. His current research interests include developing efficient, robust and implementable guidance, navigation and control (GNC) methodologies to enhance marine, land and air autonomy for science, defense, and emergency missions.

Christopher Edwards is currently a Professor of control engineering with the College of Engineering, Mathematics and Physical Sciences, University of Exeter, Exeter, U.K. His current research interests include sliding mode control and observation, and their applications. He has authored 400 refereed papers in these areas, and three books: *Sliding Mode Control: Theory and Applications* (1998), *Fault Detection and Fault Tolerant Control Using Sliding Modes* (2011), and *Sliding Mode Control and Observation* (2014), and co-edited the monograph *Fault Tolerant Flight Control: A Benchmark Challenge* (2010). He is currently the Chair of the IEEE Technical Committee on Variable Structure Systems.

Peter G. Challenor is currently a Professor of statistics with the College of Engineering, Mathematics and Physical Sciences, University of Exeter, Exeter, U.K. His current research interests include uncertainty in the natural world. These range from the statistical analysis of complex numerical models (such as those used to simulate climate) to the interpolation of noisy data and the estimation of the amount of renewable energy in the ocean. He has authored 200 refereed papers in these areas.